Cubic Pythagorean Hodograph Spline Curves and Applications to Sweep Surface Modeling

Bert Jüttler and Christoph Mäurer
Department of Mathematics
University of Technology, Darmstadt
Schloßgartenstr. 7
64289 Darmstadt, GERMANY
Phone: +49 6151 16 2789
Fax: +49 6151 16 2131
Email: juettler@mathematik.tu-darmstadt.de

This paper is devoted to cubic Pythagorean hodograph (PH) curves which enjoy a number of remarkable properties, such as polynomial arc–length function and existence of associated rational frames. Firstly we derive a construction of such curves via interpolation of G^1 Hermite boundary data with Pythagorean hodograph cubics. Based on a thorough discussion of the existence of solutions we formulate an algorithm for approximately converting arbitrary space curves into cubic PH splines, with any desired accuracy. In the second part of the paper we discuss applications to sweep surface modeling. With the help of the associated rational frames of PH cubics we construct rational representations of sweeping surfaces. We present sufficient criteria ensuring G^1 continuity of the sweeping surfaces. The paper concludes with some remarks on offset surfaces and rotation minimizing frames.

Keywords: Pythagorean hodograph curves, G^1 Hermite interpolation, spline curves, sweep surface modeling, rational frames, offset surfaces, rotation minimizing frames.

INTRODUCTION

Pythagorean Hodograph[4, 5] (PH) curves are a special class of polynomial curves. They are characterized by the fact that their hodograph (that is, their unit tangent vector $\vec{\mathbf{t}}$) corresponds to a rational curve on the unit sphere. This fact entails a number of nice properties. For instance, the arc length of a PH curve is simply a polynomial function of the curve parameter. Consequently, PH curves can be used efficiently for the numerical control of milling machines and industrial robots, where the speed control is usually based on the arc length of the trajectories[6]. Moreover, spatial PH curves can be used for creating rational sweeping surfaces, as each curve has an associated rational frame[5, 10]. Pythagorean hodograph curves have been studied in a number of publications by Farouki and coauthors[1, 3, 5]. A number of interpolation schemes for PH curves is available. The majority of these schemes, however, deals with planar data. Interpolation of planar G^1 Hermite data with planar PH quintics has been discussed by Farouki and Neff[3]. A construction for planar C^2 PH spline curves from point data has been developed by Albrecht and Farouki[1]. Recently, Meek and Walton[14] have discussed G^1 Hermite interpolation by planar PH cubics.

In the spatial case, Farouki and Sakkalis[5] describe a scheme for Hermite interpolation of C^1 boundary data (points + first derivatives) with PH quintics. Wagner and Ravani[17] have developed a method for matching spatial G^1 Hermite boundary data (points + tangents) with PH space cubics. Their approach is based on certain geometric properties of the Bézier control polygon of PH space cubics which were revealed by Farouki and Sakkalis[5]. The analysis of the existence of solutions, and of

their behaviour, however, is still somewhat incomplete. It is one of the aims of this paper to fill this gap.

In the first part of the paper we present another approach to Hermite interpolation of G^1 boundary data with spatial PH cubics. The hodographs of the PH curves are constructed at first; they describe quadratic rational curves on the unit sphere. Using a simple representation of the possible hodographs we obtain a characterization of feasible G^1 Hermite data for interpolation with PH cubics; the difference vector of the segment end points has to be contained within a certain quadratic cone which depends solely on the tangent vectors. As a consequence from this characterization of feasible data it is shown, that any space curve can be approximated by a G^1 cubic PH spline curve (i.e., a piecewise cubic PH curve whose segments are joined with continuous tangents) as accurately as desired, provided that the number of segments is chosen big enough. For the convenience of the reader, we provide a summary the G^1 Hermite interpolation scheme by Wagner and Ravani[17], as it may facilitate the implementation of the method.

In the second part of the paper we discuss the application of cubic PH spline curves to sweep surface modeling. We present a sufficient condition for G^1 spline surface and we investigate criteria that guarantee that the offsets of a sweeping surface are generated by the offset curves of the profile curve. We conclude with some comments concerning the rational approximation of the rotation minimizing frame.

BUILDING PH SPLINES

This section is devoted to Pythagorean–hodograph (PH) cubics. We discuss the approximate conversion of arbitrary space curves into a cubic PH spline curves.

PH cubics in space

Consider a cubic Bézier curve

$$\mathbf{x}(t) = \sum_{i=0}^{3} \mathbf{b}_i \, B_i^3(t), \qquad t \in [0,1], \tag{1}$$

with the control points $\mathbf{b}_i \in \mathbb{R}^3$, see Reference 9. This curve is called a Pythagorean hodograph (PH) cubic[5], if the components $\dot{x}_j(t)$ of the first derivative vector $\dot{\mathbf{x}}(t) = (d/dt)\,\mathbf{x}(t)$ satisfy the Diophantine equation

$$\dot{x}_1(t)^2 + \dot{x}_2(t)^2 + \dot{x}_3(t)^2 = p(t)^2 \tag{2}$$

for some real polynomial $p = p(t)$. That is, the quadratic polynomials $\dot{x}_1$, $\dot{x}_2$, $\dot{x}_3$ and p form a Pythagorean quadruple in the polynomial ring $\mathbb{R}$[t].

The following geometric characterization of PH cubics has been derived Farouki and Sakkalis[5]. Consider the difference vectors $\Delta\mathbf{b}_i = \mathbf{b}_i - \mathbf{b}_{i-1}$ and let $\theta_{i,j}$ be the angle between the vectors $\Delta\mathbf{b}_i$ and $\Delta\mathbf{b}_j$. Moreover, let ψ be the angle between $\Delta\mathbf{b}_1 \times \Delta\mathbf{b}_2$ and $\Delta\mathbf{b}_2 \times \Delta\mathbf{b}_3$. The Bézier curve (1) is a PH cubic if and only if the control points satisfy the conditions

$$\theta_{1,2} = \theta_{2,3} \quad \text{and} \quad \cos\psi = \frac{2\,L_2^2}{L_1 L_3} - 1 \tag{3}$$

with $L_i = \|\Delta\mathbf{b}_i\|$. These conditions entail the following formulas for the parametric speed $\sigma(t) = \|\dot{\mathbf{x}}(t)\|$ and for curvature and torsion of PH cubics:

$$\sigma(t) = 3\left(L_1\,B_0^2(t) + L_2\,\cos\theta\,B_1^2(t) + L_3\,B_2^2(t)\right),$$

$$\kappa(t) = \frac{6\,L_2\,|\sin\theta_{1,2}|}{\sigma(t)^2}, \qquad \tau(t) = \frac{-3\,L_1\,L_3\,\sin\psi}{L_2\sigma(t)^2}.$$

The ratio κ/τ is constant, hence any PH cubic is a *curve of constant slope* (also called a *cubic helix*). A thorough geometrical discussion of cubic and quartic curves with constant slope has been given by Wunderlich[19].

The Frenet–frame of a PH cubic is formed by the unit tangent $\vec{\mathbf{t}} = \dot{\mathbf{x}}(t)/\sigma(t)$, combined with the normal and binormal vectors

$$\vec{\mathbf{n}} = \frac{\sigma(t)\,\ddot{\mathbf{x}}(t) - \dot{\sigma}(t)\,\dot{\mathbf{x}}(t)}{6\,L_2\,|\sin\theta_{1,2}|\,\sigma(t)}, \quad \vec{\mathbf{b}} = \frac{\dot{\mathbf{x}}(t) \times \ddot{\mathbf{x}}(t)}{6\,L_2\,|\sin\theta_{1,2}|\,\sigma(t)} \tag{4}$$

Clearly, the three vectors are quadratic rational functions of the curve parameter t; they describe three circles on the unit sphere. The spherical part of the motion of the Frenet frame (which is given by the special orthogonal matrix $U(t) = (\,\vec{\mathbf{t}}(t)\;\vec{\mathbf{n}}(t)\;\vec{\mathbf{b}}(t)\,)$) is simply a rotation with constant axis, but varying angular velocity. PH cubics are one of the simplest representatives of curves with rational Frenet–Serret motion, the so called RF–curves. These curves have been studied recently by Wagner and Ravani[17].

In the remainder of this section we derive another characterization for PH cubics. It will be used later for discussing the existence of solutions for Hermite interpolation of G^1 boundary data.

We choose an adapted coordinate system, as follows. Let $\vec{\mathbf{t}}_0 = \Delta\mathbf{b}_1/L_1$ and $\vec{\mathbf{t}}_1 = \Delta\mathbf{b}_3/L_3$ be the unit tangent vectors of the cubic (1) at $t = 0$ and $t = 1$. We choose the direction of the z– (resp. x–) axis of the coordinate system as the bisector (resp. normal) of the tangent vectors $\vec{\mathbf{t}}_0$, $\vec{\mathbf{t}}_1$. Then, the unit tangents $\vec{\mathbf{t}}_0$, $\vec{\mathbf{t}}_1$ have the coordinates

$$\vec{\mathbf{t}}_0 = (\ 0\ s\ c\ )^\top \quad \text{and} \quad \vec{\mathbf{t}}_1 = (\ 0\ -s\ c\ )^\top \tag{5}$$

with $s = \sin\phi$, $c = \cos\phi$, where $2\,\phi = \theta_{1,3}$ is the angle between $\vec{\mathbf{t}}_0$ and $\vec{\mathbf{t}}_1$.

Lemma 1. *Let $\dot{\mathbf{x}}$ be the first derivative vector of a PH cubic with the boundary tangents (5). Then there exist parameters λ, v, $w \in \mathbb{R} \cup \{\infty\}$ such that*

$$\dot{\mathbf{x}}(t) = v^2\, B_0^2(t)\, \vec{\mathbf{t}}_0 - v\, w\, B_1^2(t) \begin{pmatrix} \lambda\, s \\ 0 \\ 1 \end{pmatrix} + w^2\, (1+\lambda^2)\, B_2^2(t)\, \vec{\mathbf{t}}_1. \tag{6}$$

Remark. The above representation uses parameters from the extended real line $\mathbb{R} \cup \{\infty\}$ in order to include the limiting case $\lambda \to \infty$ with $w\,\lambda \to \bar{w}$ ($\bar{w} \in \mathbb{R}$), hence $w \to 0$. In this case the representation (6) becomes

$$\dot{\mathbf{x}}(t) = v^2\, B_0^2(t)\, \vec{\mathbf{t}}_0 - B_1^2(t) \begin{pmatrix} v\,\bar{w}\, s \\ 0 \\ 0 \end{pmatrix} + \bar{w}^2\, B_2^2(t)\, \vec{\mathbf{t}}_1\ ; \tag{7}$$

the unit tangents $\dot{\mathbf{x}}(t)/p(t)$ form a semicircle on the unit sphere, running from $\vec{\mathbf{t}}_0$ to $\vec{\mathbf{t}}_1$.

Proof. Let

$$p(t) = q_0\, B_0^2(t) + q_1\, B_1^2(t) + q_2\, B_2^2(t) \tag{8}$$

with $q_0 = v^2$, $q_1 = -v\,w\,c$ and $q_2 = w^2\,(1+\lambda^2)$. A short computation confirms that the components of $\dot{\mathbf{x}}(t)$ satisfy the equation (2).

On the other hand, if the derivative vector of a PH cubic is given, then there exists a polynomial $p(t)$ such that $\dot{\mathbf{x}}(t)/p(t)$ is a quadratic rational curve on the unit sphere (i.e., a circular arc) which runs from $\vec{\mathbf{t}}_0$ to $\vec{\mathbf{t}}_1$. From (6) and (8) we obtain the rational Bézier curve

$$\frac{1}{p(t)}\dot{\mathbf{x}}(t) = \frac{q_0\, B_0^2(t)\, \vec{\mathbf{t}}_0 + q_1\, B_1^2(t)\, \vec{\mathbf{q}}_1 + q_2\, B_2^2(t)\, \vec{\mathbf{t}}_1}{q_0\, B_0^2(t) + q_1\, B_1^2(t) + q_2\, B_2^2(t)} \tag{9}$$

with the middle control point $\vec{\mathbf{q}}_1 = (\ \lambda\, s/c\ \ 0\ \ 1/c\ )^\top$ which describes such a circular arc. Some of these arcs running from $\vec{\mathbf{t}}_0$ to $\vec{\mathbf{t}}_1$ have been drawn in Figure 1.

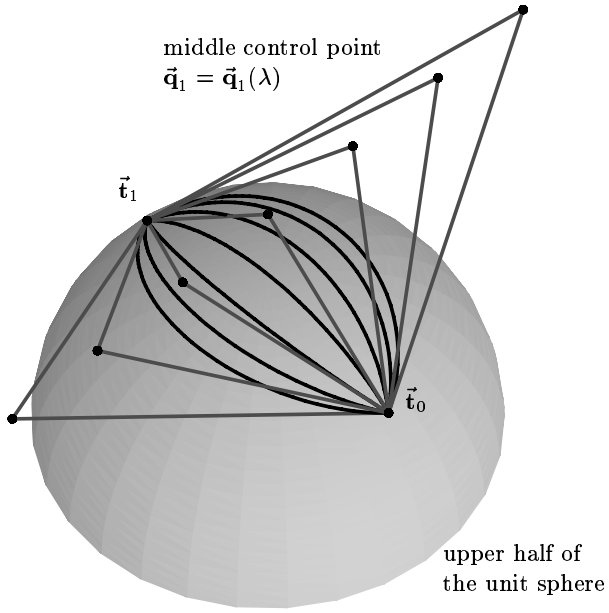

Figure 1: The normalized hodographs $\frac{1}{p(t)}\dot{\mathbf{x}}(t)$ in the standard representation (9).

All possible Bézier representations of these circular arcs can be obtained from the representation (9) by choosing the parameters λ, v, and w. This can be seen as follows. Firstly, the middle control point can be adjusted by choosing the parameter λ; it can be moved to any position along the line in which the tangent planes of the unit sphere at $\vec{\mathbf{t}}_0$ and $\vec{\mathbf{t}}_1$ intersect. In the limit $\lambda \to \infty$, the middle control point becomes a point at infinity, hence the tangent vectors form a semicircle on the unit sphere.

Secondly, the parameters v, w can be used to generate all possible normalizations and parameterizations. Note that only positive boundary weights q_0 and q_2 are possible, as the PH cubic is assumed to have the boundary unit tangents $\vec{\mathbf{t}}_0$ and $\vec{\mathbf{t}}_1$. □

Remark. The representation (6) has been constructed by applying the generalized stereographic

projection[2] δ to the system of line segments

$$v\,B_0^1(t)\begin{pmatrix}1-c\\0\\s\\0\end{pmatrix}+w\,B_1^1(t)\,(\begin{pmatrix}1-c\\0\\-s\\0\end{pmatrix}+\lambda\begin{pmatrix}0\\-s\\0\\1-c\end{pmatrix}),$$

$t\in[0,1]$. Here, these line segments are described as linear Bézier curves in so–called homogeneous coordinates. Due to space limitations we cannot discuss more details of this construction; the interested reader should consult Reference 2.

The real parameters v and w will be referred to as the *weights* of the hodograph $\dot{\mathbf{x}}(t)$. They control the length of the derivative vector, and also the distribution of the parameter t along the circular arc $\dot{\mathbf{x}}(t)/p(t)$. The parameter λ, by contrast, controls the shape of the hodograph; it specifies which one of the circular arcs running from $\vec{\mathbf{t}}_0$ to $\vec{\mathbf{t}}_1$ is taken.

Proposition 2. *Consider a PH cubic (1) with the boundary tangents (5). Then there exist parameters λ, v, $w\in\mathbb{R}\cup\{\infty\}$, such that the control points are given by the expressions*

$$\mathbf{b}_1=\mathbf{b}_0+\tfrac{1}{3}v^2\begin{pmatrix}0\\s\\c\end{pmatrix},\quad \mathbf{b}_2=\mathbf{b}_0+\tfrac{1}{3}v\begin{pmatrix}-s\,w\,\lambda\\v\,s\\v\,c-w\end{pmatrix},$$
$$\textit{and}\quad \mathbf{b}_3=\mathbf{b}_0+\tfrac{1}{3}\begin{pmatrix}-v\,s\,w\,\lambda\\s\,(-w^2+v^2-w^2\,\lambda^2)\\w^2\,\lambda^2\,c+v^2\,c+w^2\,c-v\,w\end{pmatrix}. \tag{10}$$

The first control point $\mathbf{b}_0$ is arbitrary.

Remark. As in the preceding lemma we use parameters v, w, λ from the extended real line in order to include the limit case $\lambda\to\infty$, with $w\,\lambda\to\bar{w}$ ($\bar{w}\in\mathbb{R}$), hence $w\to 0$, where one gets the control points

$$\mathbf{b}_2=\mathbf{b}_0+\tfrac{1}{3}v\begin{pmatrix}-s\,\bar{w}\\v\,s\\v\,c\end{pmatrix},\ \mathbf{b}_3=\mathbf{b}_0+\tfrac{1}{3}\begin{pmatrix}-v\,s\,\bar{w}\\s\,(v^2-\bar{w}^2)\\\bar{w}^2\,c+v^2\,c\end{pmatrix}. \tag{11}$$

Proof. These control points can easily be found by integrating the hodograph (6). The first control point $\mathbf{b}_0$ serves as the integration constant. □

With the help of this result we give a thorough discussion of the existence of solutions for Hermite interpolation of G^1 boundary data by PH cubics.

G^1 Hermite interpolation

Consider the following interpolation problem. Given the points $\mathbf{p}_0$, $\mathbf{p}_1\in\mathbb{R}^3$ and the associated unit tangent vectors $\vec{\mathbf{t}}_0$, $\vec{\mathbf{t}}_1\in\mathbb{R}^3$, find an interpolating PH cubic. That is, the PH cubic (1) is to satisfy

$$\mathbf{x}(0)=\mathbf{p}_0,\ \mathbf{x}(1)=\mathbf{p}_1,\ \dot{\mathbf{x}}(0)=\xi_0\vec{\mathbf{t}}_0,\ \text{and}\ \dot{\mathbf{x}}(1)=\xi_1\vec{\mathbf{t}}_1$$

with some positive real constants ξ_0, ξ_1. Without loss of generality one may assume that the given unit tangent vectors have the standard form (5). Moreover, we will assume that the angle between the tangents is smaller than $2\pi/3$, i.e. $\phi<\pi/3$.

Clearly, $2\pi/3=120°$ is a relatively large angle between the given tangents; it is therefore unrealistic in most applications. Hence it is well justified to concentrate on the case $\phi<\pi/3$. Later we will describe a method for converting a given space curve into a PH cubic spline curve via G^1 Hermite interpolation. In this application, the assumption $\phi<\pi/3$ can always be made true by taking more and more sample points.

As the given unit tangents are assumed to be in standard form, we can apply Proposition 2. Clearly, the PH cubic with the control points (10) matches the boundary unit tangents $\vec{\mathbf{t}}_0$ and $\vec{\mathbf{t}}_1$, provided that both weights v,w are non–zero. The first interpolation condition $\mathbf{x}(0)=\mathbf{p}_0$ is satisfied by choosing $\mathbf{b}_0=\mathbf{p}_0$. Hence, if the weights v and w and the parameter λ are chosen so that the three non–linear equations

$$\mathbf{p}_1-\mathbf{p}_0=\mathbf{b}_3-\mathbf{b}_0=\underbrace{\begin{pmatrix}-\frac{1}{3}s\,v\,w\,\lambda\\\frac{1}{3}s\,(-w^2+v^2-w^2\lambda^2)\\\frac{1}{3}\,(w^2\,\lambda^2\,c+v^2\,c+w^2\,c-w\,v)\end{pmatrix}}_{=\vec{\mathbf{q}}(v,w,\lambda)} \tag{12}$$

are satisfied, then the control points of the interpolating PH cubic can be found from Proposition 2. The solution(s) of the system (12) will be called *regular* if $v,w\neq 0$. In the limit case $\lambda\to\infty$ regular solutions are characterized by $v,\bar{w}\neq 0$. Let $\vec{\mathbf{d}}=(d_1\ d_2\ d_3)^\top=\mathbf{p}_1-\mathbf{p}_0$ be the difference vector of the given data.

Theorem 3. *The system (12) has exactly two regular real solutions (possibly including the limit case $\lambda\to\infty$, $\lambda w\to\bar{w}$) if the components of the differ-*

ence vector $\vec{\mathbf{d}}$ *satisfy the inequalities*

$$D = 4\,(1-4\,c^2)\,{d_1}^2 + (1-4\,c^2)\,{d_2}^2 + 4\,s^2\,{d_3}^2 > 0 \quad \textit{and} \quad d_3 > 0 \tag{13}$$

provided that $\vec{\mathbf{d}}$ *is neither linearly dependent on* $\vec{\mathbf{t}}_0$ *nor on* $\vec{\mathbf{t}}_1$. *If* $D = 0$ *holds, or if the difference vector is linearly dependent on one of the given unit tangents* $\vec{\mathbf{t}}_0$, $\vec{\mathbf{t}}_1$, *then there exists exactly one regular real solution. Finally, if* $D < 0$ *or* $d_3 \le 0$, *then the system has no regular real solutions.*

Proof. Any pair of weights (v, w) can be represented by

$$\begin{aligned} (v,w) &= (\,\xi\,(1-t)\,\sqrt{3},\ \xi\,t\,\sqrt{3}\,) \\ \text{or}\quad (v,w) &= (\,\xi\,(1-t)\,\sqrt{3}, -\xi\,t\,\sqrt{3}\,) \end{aligned} \tag{14}$$

with $t \in [0,1]$, $\xi \in \mathbb{R}$. The first resp. second formula applies to weights with $v\,w \ge 0$ resp. $v\,w \le 0$. In Figure 2, the above substitution is visualized by some lines t = constant and ξ = constant in the vw-plane. The dotted resp. dashed lines correspond to the first ($vw \ge 0$) resp. to the second ($vw \le 0$) substitution. The factor $\sqrt{3}$ has been introduced in order to keep the formulas in the sequel as simple as possible.

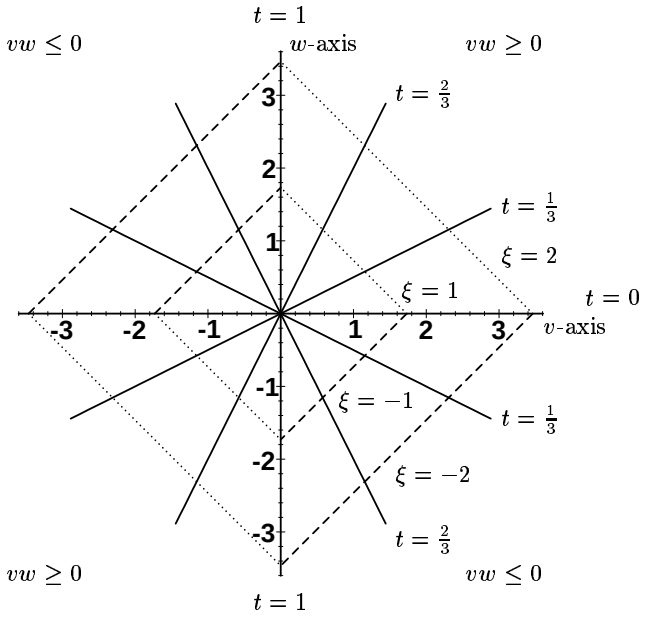

Figure 2: Weight representation, see Eq. (14).

Consider the feasible difference vectors $\vec{\mathbf{q}}(v, w, \lambda)$, see (12) for some constant λ. With the help of the above weight representation we obtain

$$\vec{\mathbf{q}}(v,w,\lambda) = \begin{cases} \xi^2\,\vec{\mathbf{r}}_1(t,\lambda) & \text{if} \quad vw \ge 0 \\ \xi^2\,\vec{\mathbf{r}}_2(t,\lambda) & \text{otherwise,} \end{cases} \tag{15}$$

where $\vec{\mathbf{r}}_{1/2}(t,\lambda)$ are the two quadratic Bézier curves

$$\begin{aligned} \vec{\mathbf{r}}_{1/2}(t,\lambda) &= B_0^2(t)\,\vec{\mathbf{t}}_0 \mp \tfrac{1}{2}\,B_1^2(t) \begin{pmatrix} s\,\lambda \\ 0 \\ 1 \end{pmatrix} \\ &+ B_2^2(t)\,(1+\lambda^2)\,\vec{\mathbf{t}}_1 \end{aligned} \tag{16}$$

with parameter $t \in [0,1]$. For $\lambda \neq 0$, both curves lie on either side of the yz–plane. For certain values of ϕ and λ, both curves and their control polygons are shown in Figure 3.

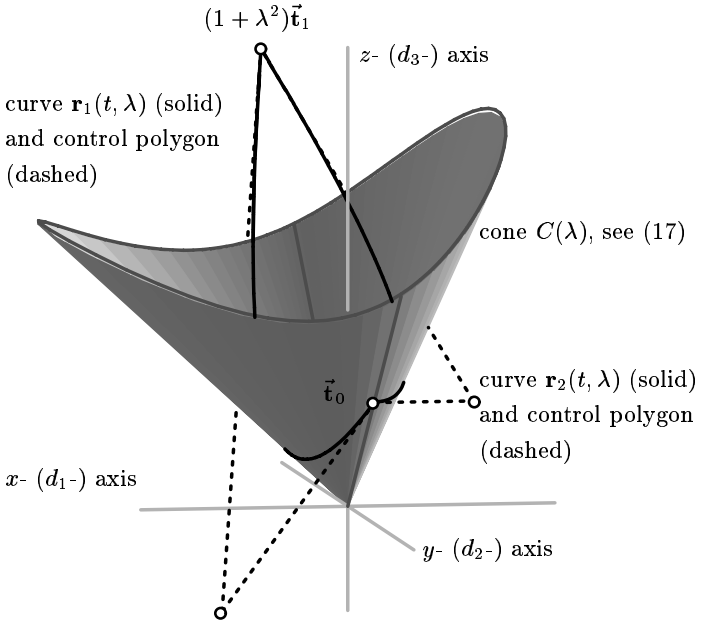

Figure 3: The cone of feasible difference vectors for $\phi = 54°$ and $\lambda = -1.5$.

Owing to (15), the set of feasible difference vectors is the collection of rays emanating from the origin which are spanned by the system of curves $\vec{\mathbf{r}}_1$, $\vec{\mathbf{r}}_2$ for λ varying in $\mathbb{R} \cup \{\infty\}$. (See the above remarks concerning the limiting case $\lambda \to \infty$.) It can easily be seen that both curves belong to the half space $z > 0$ as $\phi < \pi/3$ was assumed. Hence the feasible difference vectors satisfy the condition $d_3 > 0$.

Both curves (16) satisfy the equation

$$\vec{\mathbf{r}}_i(t,\lambda)^\top\,C(\lambda)\,\vec{\mathbf{r}}_i(t,\lambda) = 0; \quad i = 1,2,$$

with the 3×3–matrix

$$C(\lambda) = \begin{pmatrix} 4c^2 + 4c^2\lambda^2 - 1 & 0 & s\lambda \\ 0 & c^2\lambda^2 & 0 \\ s\lambda & 0 & -s^2\lambda^2 \end{pmatrix}.$$

Hence, for any constant value $\lambda = \lambda_0$ with $\lambda_0 \neq 0$, the feasible difference vectors form the upper half ($d_3 \ge 0$) of the quadratic cone

$$\vec{\mathbf{d}}^\top\,C(\lambda)\,\vec{\mathbf{d}} = 0, \tag{17}$$

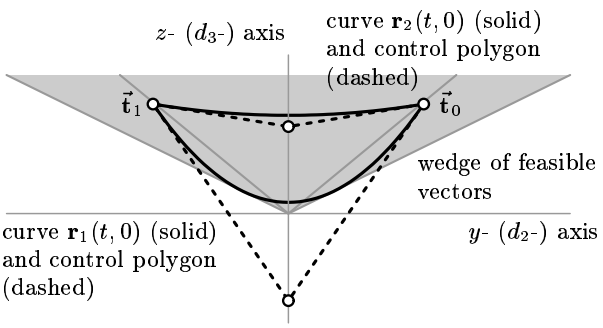

Figure 4: The case $\lambda = 0$.

see again Figure 3, where this cone has been drawn as far as it is contained within the sphere with radius 2. Clearly, the rays spanned by the two curves $\vec{\mathbf{r}}_{1/2}(t, \lambda_0)$ cover the whole upper half of the cone (17), as both curves lie on either side of the yz–, but on the same side of the xy–plane. The equation of the cone (17) has been constructed by implicitizing the expression $\vec{\mathbf{q}}(v, w, \lambda)$ with respect to the weights v, w, cf. 9.

In the case $\lambda_0 = 0$ both curves $\vec{\mathbf{r}}_{1/2}(t, 0)$ belong to the yz–plane. This situation is illustrated by Figure 4. The set of feasible vectors is the wedge which is bounded by the tangents to $\vec{\mathbf{r}}_1(t, 0)$ passing through the origin. A short calculation leads to the directions of these extreme rays,

$$(\, 0 \quad \pm 2\, s \quad \sqrt{4\, c^2 - 1} \,)^\top. \tag{18}$$

If λ varies in $\mathbb{R} \cup \{\infty\}$, then the upper halves of the quadratic cones (17) and the wedge obtained for $\lambda_0 = 0$ form the set of all points which satisfy the conditions $D \geq 0$ and $d_3 \geq 0$, cf. (13). This can be seen as follows. An arbitrary vector $\vec{\mathbf{d}} = (\, d_1 \; d_2 \; d_3 \,)^\top$ which is not contained in the yz–plane (i.e. $d_1 \neq 0$) belongs to one of the cones (17), if and only if the quadratic equation $\vec{\mathbf{d}}^\top C(\lambda) \, \vec{\mathbf{d}} = 0$ for the parameter λ has got real solutions. Factoring the discriminant of this quadratic equation immediately gives the condition $D \geq 0$. Moreover, the intersection of the yz–plane with the quadratic cone $D = 0$ produces exactly the wedge of feasible difference vectors for $\lambda = 0$, cf. (18). Hence, the feasible difference vectors $\vec{\mathbf{d}} = (\, d_1 \; d_2 \; d_3 \,)$ satisfy the conditions $D \geq 0$ and $d_3 \geq 0$.

We conclude the proof by discussing the number of regular solutions.

Case 1. If $\vec{\mathbf{d}}$ is not contained in the yz–plane and $D > 0$ holds, then (17) has two solutions $\lambda_1, \lambda_2 \neq 0$, hence we get two solutions (λ_1, v_1, w_1) and (λ_2, v_2, w_2). (If the left–hand side of (17) degenerates into a linear (resp. constant) expression, then $\lambda = \infty$ is to be considered as a single (resp. double) root.) The weights v_i, w_i associated with the solutions λ_i can be found by intersecting the ray spanned by $\vec{\mathbf{d}}$ with the curves $\vec{\mathbf{r}}_{1/2}(t, \lambda_j)$, $j = 1, 2$, $t \in [0, 1]$. For each λ_j, exactly one of both curve segments intersects the ray. The scaling factor ξ^2 can then be chosen so that the PH cubic matches the given difference vector $\vec{\mathbf{d}}$. Note that the parameters $(\lambda, \pm v, \pm w)$ produce the same PH cubic. Finally, both solutions are guaranteed to be regular, as $w = 0$ (resp. $v = 0$) entails linear dependency of $\vec{\mathbf{d}}$ and $\vec{\mathbf{t}}_1$ (resp. $\vec{\mathbf{t}}_2$). This, however, is impossible as $\vec{\mathbf{d}}$ was assumed to be outside of the yz–plane.

Case 2. If $\vec{\mathbf{d}}$ is not contained in the yz–plane and $D = 0$ holds, then (17) has only one solution $\lambda = \lambda_0$. The same arguments as in the first case prove that this solution leads to exactly one regular interpolating PH cubic.

Case 3. If $\vec{\mathbf{d}}$ is contained in the yz–plane, then regular solutions can only be obtained from $\lambda = 0$. (Solutions with $\lambda \neq 0$ are only possible, if $\vec{\mathbf{d}}$ is linearly dependent on $\vec{\mathbf{t}}_1$ or $\vec{\mathbf{t}}_2$. In both cases, however, one would get solutions with either $v = 0$ or $w = 0$.) The number of regular solutions with $\lambda = 0$ can be seen from Figure 4 by counting the number of intersections of the ray spanned by $\vec{\mathbf{d}}$ with the curves $\vec{\mathbf{r}}_{1/2}(t, 0)$. Intersections at the segment boundaries of both curves ($t = 0$ or $t = 1$) correspond to degenerate solutions (cf. (14)), but intersections at the interior yield regular ones. If $D > 0$ holds and $\vec{\mathbf{d}}$ is neither linearly dependent on $\vec{\mathbf{t}}_1$ nor on $\vec{\mathbf{t}}_2$, then there exist two regular solutions. If $D = 0$, or if $\vec{\mathbf{d}}$ is either linearly dependent on $\vec{\mathbf{t}}_1$ or on $\vec{\mathbf{t}}_2$, then there exists only one regular solution. □

Finally we outline a geometric interpretation of the above result. Consider the family of quadratic cones (17) with the parameter $\lambda \in \mathbb{R} \cup \{\infty\}$. It is visualized in Figure 5. Instead of the quadratic cones themselves, we have simply drawn the spherical curves (thin black lines) which are obtained by intersecting them with the unit sphere. For $\lambda \neq 0$ this produces oval curves; $\lambda = 0$ gives a circular arc. All curves (hence all the cones (17)) pass through the given tangent directions $\vec{\mathbf{t}}_0$, $\vec{\mathbf{t}}_1$ (shown as dotted

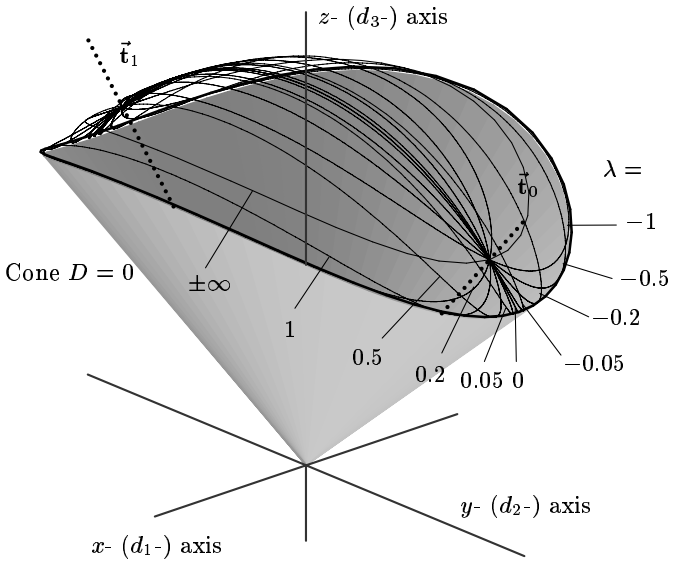

Figure 5: The quadratic cone $D = 0$ is enveloped by the family of cones (17).

lines). The quadratic cone $D = 0$ is the envelope of the family (17). It can clearly be seen from the figure that the family of cones covers the whole interior of the cone $D = 0$; hence difference vectors with $D \geq 0$ and $d_3 > 0$ admit solutions of the G^1 Hermite interpolation problem.

Summing up, if the difference vector belongs to the interior of the quadratic cone D, then regular real solution to the G^1 Hermite interpolation problem are guaranteed to exist. The quadratic cone depends solely on the given tangent directions $\vec{\mathbf{t}}_0$, $\vec{\mathbf{t}}_1$. The rays spanned by the tangent directions are contained within the cone D.

Computing the solutions

The solutions of the G^1 Hermite interpolation could be computed via the non-linear system (12)[10]. For the implementation it may be easier to use an alternative approach developed by Wagner and Ravani[17]. The following algorithm is equivalent to their formulas:

- Synopsis. Geometric Hermite interpolation with spatial PH cubics.

1. Input: Boundary Bézier points $\mathbf{p}_0 = \mathbf{b}_0$, $\mathbf{p}_1 = \mathbf{b}_3$ and associated unit tangents $\vec{\mathbf{t}}_0$, $\vec{\mathbf{t}}_1$.

2. $\mathbf{m}_1 := (\vec{\mathbf{t}}_0 \cdot \vec{\mathbf{t}}_1)\,\vec{\mathbf{t}}_1 - \vec{\mathbf{t}}_0$, $\mathbf{m}_2 := \vec{\mathbf{t}}_1 - (\vec{\mathbf{t}}_0 \cdot \vec{\mathbf{t}}_1)\,\vec{\mathbf{t}}_0$

3. $\lambda_1 := \dfrac{\mathbf{m}_1 \cdot (\mathbf{b}_3 - \mathbf{b}_0)}{\mathbf{m}_1 \cdot \mathbf{t}_0}$, $\lambda_2 := \dfrac{\mathbf{m}_2 \cdot (\mathbf{b}_0 - \mathbf{b}_3)}{\mathbf{m}_2 \cdot \mathbf{t}_1}$

4. $\mathbf{n}_1 := \mathbf{b}_0 + \lambda_1 \vec{\mathbf{t}}_1$, $\mathbf{n}_2 := \mathbf{b}_3 + \lambda_2 \vec{\mathbf{t}}_1$

5. Solve the quadratic equation

$$(|\lambda_1| - X)(|\lambda_2| - X) - 4X^2 \frac{1 + \vec{\mathbf{t}}_0 \cdot \vec{\mathbf{t}}_1}{2} = \frac{2\|\mathbf{n}_1 - \mathbf{n}_2\|^2}{1 - \vec{\mathbf{t}}_0 \cdot \vec{\mathbf{t}}_1} \tag{19}$$

for the unknown X.

6. Output: Inner Bézier points (2 solutions) $\mathbf{b}_1 = \mathbf{n}_1 - X_{1/2}\,\vec{\mathbf{t}}_0$, $\mathbf{b}_2 = \mathbf{n}_2 + X_{1/2}\,\vec{\mathbf{t}}_1$

The algorithm computes the unknown Bézier points $\mathbf{b}_1$ and $\mathbf{b}_2$ of the PH cubic to given Hermite data. Note that the quadratic equation (19) does not always have real solutions. Also, even if real solutions $X_{1/2}$ exist, it may happen that the interpolating PH cubic matches the unit tangents $\vec{\mathbf{t}}_0$, $\vec{\mathbf{t}}_1$ with the opposite orientation. Finally, if real solutions with the correct orientation at the boundaries exist, then one will get two different solutions in general, owing to the possibly different roots of (19). One should then pick the solutions with the shorter control polygon.

In the original paper by Wagner and Ravani[17], the questions of solvability and suitability of the solutions have not been discussed in much detail. As observed there, real solutions to (19) are guaranteed to exist provided that the angle between the given unit tangents is bigger than $2\pi/3$. This situation is rather unrealistic situation in applications. However, even in this case it is not clear whether the solutions will match the given tangent data with the desired orientation.

Necessary and sufficient criteria for the existence of regular real solutions having the desired orientation are provided by Theorem 3. In order to apply this result, however, the given unit tangents have to be converted into the standard form (5). In the next section we discuss the approximate conversion of space curves into cubic PH splines via the above G^1 Hermite interpolation procedure. Also, we will discuss the behaviour of the two different solutions.

Approximate conversion of space curves

Consider a given space curve segment $\mathbf{p} = \mathbf{p}(t)$ with the parameter t varying in the interval $[0, S]$. One may assume that the parameter t is the arc length of

the curve, i.e. $\|\vec{\mathbf{t}}(t)\| = \|\dot{\mathbf{p}}(t)\| \equiv 1$ holds, see Reference 13. With the help of the above G^1 Hermite interpolation procedure, we want to approximate the given curve with a sequence of PH cubics. Firstly, for a given stepsize $\Delta = S/N$, we generate a sequence of points $\mathbf{p}(i\,\Delta)$ with associated unit tangent vectors $\vec{\mathbf{t}}(i\,\Delta)$, $i = 0, \ldots, N$. Secondly, we apply the above–described Hermite interpolation procedure to each pair of adjacent G^1 Hermite data $\mathbf{p}(i\,\Delta), \vec{\mathbf{t}}(i\,\Delta)$ and $\mathbf{p}(\,(i{+}1)\,\Delta), \vec{\mathbf{t}}(\,(i{+}1)\,\Delta)$. If the assumptions of Theorem 3 are satisfied for each segment, then this leads to a PH cubic spline curve. In the sequel we discuss the following question.

Is it always possible to convert the given curve $\mathbf{p}(t)$ *into a cubic PH spline with any desired accuracy via* G^1 *Hermite interpolation?*

In order to answer this question, one has to discuss the asymptotic behaviour of the solutions to the Hermite interpolation problem for $\Delta \to 0$. We consider the given curve in a neighbourhood of a point $\mathbf{p}(t_0)$. Under suitable assumptions about its differentiability, the curve can be represented by its canonical Taylor expansion

$$\mathbf{p}(t) = \begin{pmatrix} (t{-}t_0) - \frac{1}{6}\,\kappa_0^2\,(t{-}t_0)^3 + \ldots \\ \frac{1}{2}\,\kappa_0\,(t{-}t_0)^2 + \frac{1}{6}\,\kappa_1\,(t{-}t_0)^3 + \ldots \\ \frac{1}{6}\,\kappa_0\,\tau_0\,(t{-}t_0)^3 + \ldots \end{pmatrix}$$

which results from the well–known Frenet formulas, see any textbook on differential geometry[13]. Here, the origin of the coordinate system is at $\mathbf{p}(t_0)$, the p_1–axis is spanned by $\vec{\mathbf{t}}(t_0)$, and the p_1p_2–plane is the osculating plane of the curve at $\mathbf{p}(t_0)$. The coefficients κ_i, τ_j are the derivatives of curvature and torsion at $t = t_0$,

$$\kappa_i = \left.\frac{d^i}{dt^i}\kappa(t)\right|_{t=t_0} \quad \text{and} \quad \tau_j = \left.\frac{d^j}{dt^j}\tau(t)\right|_{t=t_0}.$$

The curve points $\mathbf{p}(t_0)$, $\mathbf{p}(t_0+\Delta)$ with the associated unit tangent vectors $\vec{\mathbf{t}}(t_0)$, $\vec{\mathbf{t}}(t_0+\Delta)$ are to be interpolated with a PH cubic.

Firstly, in order to apply the formulas from the previous section, we have to transform the data into the local coordinate system. Its x_1–axis (resp. x_3–axis) has the direction $\vec{\mathbf{t}}(t_0)\times\vec{\mathbf{t}}(t_0+\Delta)$ (resp. $\vec{\mathbf{t}}(t_0)+\vec{\mathbf{t}}(t_0+\Delta)$). With the help of computer algebra tools one gets Taylor expansions for $c = \cos\phi$, $s = \sin\phi$, and for the components of the difference vector $\vec{\mathbf{d}} = \mathbf{p}(t_0+\Delta) - \mathbf{p}(t_0)$ of the segment end points:

$$\begin{aligned} c &= 1 - \tfrac{1}{8}\,\kappa_0^2\,\Delta^2 - \tfrac{1}{8}\,\kappa_0\,\kappa_1\,\Delta^3 + \ldots, \\ s &= \tfrac{1}{2}\,\kappa_0\,\Delta + \tfrac{1}{4}\,\kappa_1\,\Delta^2 \\ &\qquad + \tfrac{1}{12}\,(\kappa_2 - \tfrac{1}{4}\,\kappa_0\,\tau_0^2 - \tfrac{1}{4}\,\kappa_0^3)\,\Delta^3 + \ldots, \\ d_1 &= \tfrac{1}{12}\,\kappa_0\,\tau_0\,\Delta^3 + \ldots, \\ d_2 &= \tfrac{11}{12}\,\kappa_1\,\Delta^3 + \ldots \quad \text{and} \\ d_3 &= \Delta - \tfrac{1}{24}\,\kappa_0^2\Delta^3 + \ldots. \end{aligned}$$

Now we can check whether the conditions of Theorem 3 become true if the stepsize Δ converges to zero. Obviously, the second condition $d_3 > 0$ gets true for sufficiently small stepsize Δ. On the other hand, the left–hand side of the first inequality from (13) has the Taylor expansion

$$\begin{aligned} D = {\kappa_0}^2\Delta^4 + \kappa_0\,\kappa_1\,\Delta^5 + (&-\tfrac{1}{6}{\kappa_0}^2\tau_0^2 \\ &-\tfrac{1}{6}{\kappa_0}^4 + \tfrac{11}{48}{\kappa_1}^2 + \tfrac{1}{3}\kappa_0\,\kappa_2)\Delta^6 + \ldots \end{aligned} \tag{20}$$

If the curve has non–zero curvature at $\mathbf{p}(t_0)$ (i.e., $\kappa_0 \neq 0$), then this expression is guaranteed to be positive for sufficiently small stepsize Δ. We give a brief geometric interpretation of this fact. Consider the angle between the difference vector $\vec{\mathbf{d}}$ and the z–axis of the local coordinate system. It can be shown to converge *quadratically* to zero. On the other hand, consider the apex angles (there are two extreme apex angles, as the cone is not a circular one) of the quadratic cone $D = 0$ (see Figure 5) of the feasible difference vectors. Both apex angles converge *linearly* to zero for $\Delta \to 0$. Thus, if the stepsize is small enough, then the cone of feasible vectors is guaranteed to contain the difference vector of the data. For more details the reader is referred to 10.

Now we consider the case $\kappa_0 = 0$. That is, the original curve has got an inflection or a flat point at $t = t_0$. Similar to the previous case, we consider the Taylor expansion of the left–hand side of the first inequality (13). This leads to $\frac{11}{48}{\kappa_1}^2\Delta^6 + \ldots$. Thus, even in this case we are guaranteed to find real solutions, provided that the stepsize is sufficiently small. We presume (and this is supported by our numerical experiments) that this fact applies to arbitrary space curves. For the proof of this conjecture one would simply have to consider the higher order terms of the Taylor expansion (20).

If the input curve is given as a parametric cubic spline curve (which is of course a standard repre-

sentation in CAD systems), then input curves with both $\kappa_0 = \kappa_1 = 0$ can be shown to be segments of straight lines. That is, the G^1 interpolation procedure is guaranteed to be successful for cubic splines as input curves, provided that the stepsize is sufficiently small.

Next we summarize some results concerning the asymptotic behaviour of the solutions for decreasing stepsize $\Delta \to 0$. For more details the reader should consult Reference 10. If the stepsize is sufficiently small, then the G^1 interpolation procedure will produce two different solutions. Their control points can be represented as

$$\mathbf{b}_0 = \mathbf{p}(t_0), \quad \mathbf{b}_1 = \mathbf{p}(t_0) + l_{1,i}\,\vec{\mathbf{t}}(t_0),$$
$$\mathbf{b}_2 = \mathbf{p}(t_0{+}\Delta) - l_{2,i}\,\vec{\mathbf{t}}(t_0{+}\Delta), \text{ and } \mathbf{b}_3 = \mathbf{p}(t_0{+}\Delta),$$

$i = 1, 2$, with certain lengths $l_{1,i}$, $l_{2,i}$. If we use the first solution (the one with the short control polygon, see the previous section), then both lengths can be shown to be asymptotically equal to $l_{1,1} = l_{2,1} = (1/3)\Delta + \ldots$. For this solution, the length of the spherical curve (9) which is formed by the unit tangent vectors of the interpolating PH cubic tends to zero. For decreasing stepsize $\Delta \to 0$, the first solution converges to the solution of C^1 Hermite interpolation with standard cubic Bézier curves, where the given curve $\mathbf{p}(t)$ is parameterized with respect to its arc length.

For the second solution, by contrast, we get $l_{1,2} = l_{2,2} = \Delta + \ldots$. In this case, the length of the spherical curve (9) which is formed by the unit tangent vectors converges to $2\,\pi$. The first solution is to be preferred, as the shape of the resulting spline curves is much better.

The asymptotic behaviour of both solutions is depicted in Figure 6. The original curve segment has been drawn in grey. The solid (resp. dashed) curve show the cubic Bézier curve which is obtained from the first (resp. second) solution of the G^1 Hermite interpolation problem.

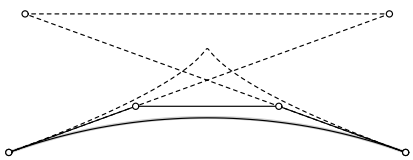

Figure 6: Asymptotic behaviour of the two solutions (schematic).

For each point $\mathbf{p}(t_0)$ of the given curve we can find a maximum stepsize $\Delta_{\max}(t_0)$, such that the solution to the Hermite interpolation problem with the point and tangent data $\mathbf{p}(t_0)$, $\mathbf{p}(t_0 + \Delta)$ and $\vec{\mathbf{t}}(t_0)$, $\vec{\mathbf{t}}(t_0 + \Delta)$ exists for any stepsize $\Delta \in [0, \Delta_{\max}(t_0)]$. Clearly, the maximum stepsize at each point is positive. Hence there exists a global lower bound Δ_0 for the maximum stepsize, as we are dealing with a curve segment of finite length S. Summing up, we have the following result:

Consider a given curve segment $\mathbf{p}(t)$, $t \in [0, S]$ of finite length which is sufficiently often differentiable or which is a collection of segments which are sufficiently often differentiable. (The latter assumption is satisfied by the curve representations of CAD systems.) *With the help of G^1 Hermite interpolation with PH cubics as described in the previous section, this curve can be approximately converted into a PH cubic spline curve. By increasing the number of segments, the approximation can be made as highly accurate as desired.*

For practical implementations, one should use an adaptive choice of the stepsize, in order to keep the number of segments as small as possible. This is described in the following algorithm (see also the remarks below).

- SYNOPSIS. Approximate conversion of a space curve into a PH cubic spline curve.

1. INPUT. Original curve $\mathbf{p}(t)$, parameterized by its arc–length ($\|\dot{\mathbf{p}}(t)\| \equiv 1$); tolerance ϵ.
2. Find all points with vanishing curvature $\kappa(t) = \|\ddot{\mathbf{p}}(t)\|$ and split the curve into segments with non–zero curvature in the interior. Apply step 3 to all these segments.
3. Conversion of a curve segment $\mathbf{p}(t)$, with $t \in [t_0, t_1] \subseteq [0, S]$.
   - 3.1 Apply the G^1 Hermite interpolation procedure (see previous section) to the boundary data $\mathbf{p}_0 = \mathbf{p}(t_0)$, $\mathbf{p}_1 = \mathbf{p}(t_1)$ with tangents $\vec{\mathbf{t}}_0 = \dot{\mathbf{p}}(t_0)$, $\vec{\mathbf{t}}_1 = \dot{\mathbf{p}}(t_1)$.
   - 3.2 Check whether the PH cubic obtained from the previous step approximates the original curve with the desired accuracy. If yes: return. Otherwise: split the curve into halves $t \in [t_0, \frac{t_0+t_1}{2}]$ and $t \in [\frac{t_0+t_1}{2}, t_1]$ and apply step 3 to both segments.

4. OUTPUT. Sequence of cubic PH curves, forming a G^1 spline curve.

Remarks. Step 1. Clearly, the original curve will almost never be given by its arc–length parameterization. However, in order to get a geometrically invariant conversion procedure (which does not depend on the parameterization of the input curve), the original curve should (at least approximately) be parameterized by its arc length. Recently, an efficient algorithm for computing the arc length of Bézier curves has been developed by Gravesen[7].

Step 2. Splitting the curve at points with vanishing curvature is not required in order to guarantee the existence of solutions, but it will improve the shape of the resulting PH spline curve; it avoids PH cubics whose unit tangents form a circular arc with a large vertex angle. For true space curves it is very unlikely to find points with vanishing curvature. This, however, is very different in the planar case, where those points (inflections or flat points) may occur quite frequently.

Step 3.2. The check for the accuracy of the approximation has to be done numerically as well. For instance, the maximum of the function

$$\|\mathbf{x}(t) - \mathbf{p}(t_0\,(1-t) + t_1\,t)\|, \quad t \in [0,1],$$

gives an upper bound for the distance error between the curve $\mathbf{p}(t)$ and the approximating PH cubic $\mathbf{x}(t)$.

An illustration of the output of the algorithm – together with a generated sweeping surface – is provided in the final section of the paper (Figure 8).

The above conversion procedure generalizes an interpolation scheme by Meek and Walton[14] to the spatial situation. In the planar case it has been shown[14] that the error behaves asymptotically like $O(\Delta^4)$. So far we have not succeeded to generalize the error analysis to the spatial case, due to the more complex formulas for computing the solutions. This will be a matter of future research.

SURFACE APPLICATIONS

A main advantage of PH curves is that they possess rational frames[5, 10]. This property can be used to derive exact rational parameter representations of sweeping surfaces and skinning surfaces, to describe rational motions in robotics, or for the generalized cylinder technique in computer animation. In this section we will discuss rational representations and properties of sweeping surfaces with a cubic PH spine curve.

Rational frames of PH cubics

A moving frame of a space curve $\mathbf{x}(t)$ can be defined with the orthogonal unit vectors $\{\vec{\mathbf{f}}_1(t), \vec{\mathbf{f}}_2(t), \vec{\mathbf{f}}_3(t)\}$. We assume that $\vec{\mathbf{f}}_1(t) := \dot{\mathbf{x}}(t)/\|\dot{\mathbf{x}}(t)\|$ is the unit tangent vector of the spine curve $\mathbf{x}(t)$. Therefore $\vec{\mathbf{f}}_2(t)$ and $\vec{\mathbf{f}}_3(t)$ span the normal plane of $\mathbf{x}(t)$. It is convenient to describe the frame vectors in relation to the Frenet frame as

$$\begin{aligned} \vec{\mathbf{f}}_2(t) &= \sin\Omega(t)\,\vec{\mathbf{b}}(t) + \cos\Omega(t)\,\vec{\mathbf{n}}(t) \\ \vec{\mathbf{f}}_3(t) &= \cos\Omega(t)\,\vec{\mathbf{b}}(t) - \sin\Omega(t)\,\vec{\mathbf{n}}(t), \end{aligned} \quad (21)$$

where the normal and the binormal of the cubic are given by (4). Substituting $w(t) = \tan(\Omega(t)/2)$ we obtain a rational frame representation

$$\begin{aligned} \vec{\mathbf{f}}_2(t) &= \frac{2w(t)}{1+w^2(t)}\,\vec{\mathbf{b}}(t) + \frac{1-w^2(t)}{1+w^2(t)}\,\vec{\mathbf{n}}(t) \\ \vec{\mathbf{f}}_3(t) &= \frac{1-w^2(t)}{1+w^2(t)}\,\vec{\mathbf{b}}(t) - \frac{2w(t)}{1+w^2(t)}\,\vec{\mathbf{n}}(t) \end{aligned} \quad (22)$$

of degree $2(1+n)$, where n is the degree of the polynomial or rational function $w(t)$. A planar (at least G^1-continuous) cross section curve $\mathbf{c}(s) = (c_1(s), c_2(s))^T$ of degree m in the normal plane of $\mathbf{x}(t)$ defines a rational sweeping surface

$$\mathbf{s}(s,t) = \mathbf{x}(t) + \vec{\mathbf{f}}_2(t)\;c_1(s) + \vec{\mathbf{f}}_3(t)\;c_2(s) \quad (23)$$

of degree $(m, 2n+5)$.

Continuity of sweeping surfaces

If two PH cubics $\mathbf{x}^-(t)$ and $\mathbf{x}^+(t)$, $t \in [0,1]$ are joined G^1-continuous at $\mathbf{x}^-(1) = \mathbf{x}^+(0)$, the corresponding sweeping surface patches $\mathbf{s}^-(s,t)$ and $\mathbf{s}^+(s,t)$ $s,t \in [0,1]$ should be G^1-continuous along there common boundary curve $\mathbf{s}^-(s,1) = \mathbf{s}^+(s,0)$, too. In order to guarantee G^1-continuity, we derive a sufficient condition for the functions $\Omega(t)$ and $w(t)$.

Firstly we consider the continuity of the frame vectors $\mathbf{f}_2$ and $\mathbf{f}_3$. The conditions

$$\vec{\mathbf{f}}_2^{\,-}(1) = \vec{\mathbf{f}}_2^{\,+}(0)\ ,\ \vec{\mathbf{f}}_3^{\,-}(1) = \vec{\mathbf{f}}_3^{\,+}(0)$$

describe the G^0-continuity. In order to obtain G^1-continuity, the frame vectors have to satisfy the

equations

$$\frac{d}{dt}\vec{\mathbf{f}}_2^{\,-}(1) = \mu\ \frac{d}{dt}\ \vec{\mathbf{f}}_2^{\,+}(0)\ ,\ \ \frac{d}{dt}\vec{\mathbf{f}}_3^{\,-}(1) = \mu\ \frac{d}{dt}\ \vec{\mathbf{f}}_3^{\,+}(0), \tag{24}$$

with an arbitrary constant $\mu \neq 0$. Generally, the Frenet frame of a cubic PH spline is not G^0! We will describe the relation between the Frenet frames at the joint boundary of two PH cubics with

$$\begin{aligned} \vec{\mathbf{n}}^{\,+}(0) &= \sin\delta\ \vec{\mathbf{b}}^{\,-}(1) + \cos\delta\ \vec{\mathbf{n}}^{\,-}(1) \\ \vec{\mathbf{b}}^{\,+}(0) &= \cos\delta\ \vec{\mathbf{b}}^{\,-}(1) - \sin\delta\ \vec{\mathbf{n}}^{\,-}(1). \end{aligned} \tag{25}$$

Now we formulate the continuity conditions for the frame vectors.

Theorem 4. *The frame vectors* $\vec{\mathbf{f}}_i^{\,-}$ *and* $\vec{\mathbf{f}}_i^{\,+}$ $(i = 2, 3)$ *of two* G^1*-continuous PH cubics* $\mathbf{x}^-(t)$ *and* $\mathbf{x}^+(t)$ *are joined* G^0*-continuous if the angle functions* $\Omega^-(t)$ *and* $\Omega^+(t)$ *satisfy*

$$\Omega^-(1) = \Omega^+(0) + \delta. \tag{26}$$

They are G^1*-continuous if additionally the relation*

$$\begin{aligned} &[\tau^+(0)\,\sigma^+(0) + \dot{\Omega}^+(0)]\ \sigma^-(1)\,\kappa^-(1)\cos\Omega^-(1) \\ &= [\tau^-(1)\,\sigma^-(1) + \dot{\Omega}^-(1)]\ \sigma^+(0)\,\kappa^+(0)\cos\Omega^+(0) \end{aligned} \tag{27}$$

is fulfilled.

Proof. It is sufficient to prove the result for the frame vector $\vec{\mathbf{f}}_2$; the G^0-condition (26) can be obtained directly by combining the equations (21) and (25). Using

$$\begin{aligned} \frac{d}{dt}\ \vec{\mathbf{f}}_2(t) &= -\kappa(t)\cos\Omega(t)\dot{\mathbf{x}}(t) \\ &+[\tau(t)\|\dot{\mathbf{x}}(t)\| + \dot{\Omega}(t)]\ [\cos\Omega(t)\vec{\mathbf{b}}(t) - \sin\Omega(t)\vec{\mathbf{n}}(t)] \end{aligned} \tag{28}$$

the boundary derivatives can be rewritten as

$$\begin{aligned} \frac{d}{dt}\vec{\mathbf{f}}_2^{\,-}(1) &= -\kappa^-(1)\cos\Omega^-(1)\dot{\mathbf{x}}^-(1) \\ &+[\tau^-(1)\sigma^-(1) + \dot{\Omega}^-(1)] \\ &\quad\times[\cos\Omega^-(1)\vec{\mathbf{b}}^{\,-}(1) - \sin\Omega^-(1)\vec{\mathbf{n}}^{\,-}(1)] \end{aligned}$$

$$\begin{aligned} \frac{d}{dt}\vec{\mathbf{f}}_2^{\,+}(0) &= -\kappa^+(0)\cos\Omega^+(0)\dot{\mathbf{x}}^+(0) \\ &+[\tau^+(0)\sigma^+(0) + \dot{\Omega}^+(0)] \\ &\quad\times[\cos\Omega^-(1)\vec{\mathbf{b}}^{\,-}(1) - \sin\Omega^-(1)\vec{\mathbf{n}}^{\,-}(1)] \end{aligned}$$

Hence,

$$\begin{aligned} \kappa^-(1)\cos\Omega^-(1)\,\sigma^-(1) &= \mu\,\kappa^+(0)\cos\Omega^+(0)\,\sigma^+(0) \\ \tau^-(1)\,\sigma^-(1) + \dot{\Omega}^-(1) &= \mu\,[\tau^+(0)\,\sigma^+(0) + \dot{\Omega}^+(0)]. \end{aligned}$$

The relation (27) is now obtained by eliminating the parameter μ. □

The G^1-continuity of the frame vectors guarantees the G^1-continuity of the trajectories of the corresponding sweeping surface and therefore the G^1-continuity of the sweeping surface itself. Substituting $w(t) = \tan(\Omega(t)/2)$ we may formulate the following sufficient G^1-condition for rational sweeping surfaces:

Corollary 5. *Let* $\mathbf{s}^-(s,t)$ *and* $\mathbf{s}^+(s,t)$ $\ s,t \in [0,1]$ *be two rational sweeping surface patches of the form (23), with* G^1*-continuous spine curves* $\mathbf{x}^-(t)$ *and* $\mathbf{x}^+(t)$ $\ t \in [0,1]$. *If the functions* $w^-(t)$ *and* $w^+(t)$ *in (22) satisfy the equations*

$$2\arctan(w^-(1)) = 2\arctan(w^+(0)) + \delta, \tag{29}$$

$$\begin{aligned} &[\tau^+(0)\,\sigma^+(0)(1+w^+(0)^2) + 2\dot{w}^+(0)] \\ &\qquad \sigma^-(1)\,\kappa^-(1)(1+w^-(1)^2)^2 \\ &= [\tau^-(1)\,\sigma^-(1)(1+w^-(1)^2) + 2\dot{w}^-(1)] \\ &\qquad \sigma^+(0)\,\kappa^+(0)(1+w^+(0)^2)^2, \end{aligned} \tag{30}$$

then the patches are joined G^1*-continuous along the curve* $\mathbf{s}^-(s,1) = \mathbf{s}^+(s,0)$. *In particular, the isoparametric curves* s*=const. are* G^1*-continuous.*

If the boundary data $w^-(1)$ and $\dot{w}^-(1)$ of the left segment are given, the corresponding boundary data $w^+(0)$ and $\dot{w}^+(0)$ can be computed via the linear equations (29) and (30). For $w(t) = \text{const.}$ in each interval the rational sweeping surface is generated with a frame parallel to the Frenet frame and has the degree (m,5). Since (30) is not always satisfied, the sweeping surface is in general along the segment boundaries just G^0-continuous (see Figure 7, top). In order to built a G^1-continuous sweeping surface one needs an at least piecewise linear function $w(t)$. In this case we obtain patches of degree $(m,7)$ (see Figure 7, bottom).

Offsetting

The offset surface $\mathbf{s}_o$ of a surface is defined as

$$\mathbf{s}_o(s,t) = \mathbf{s}(s,t) + d\frac{\mathbf{N}(s,t)}{\|\mathbf{N}(s,t)\|}\ ,\ \ d \in \mathbb{R}.$$

The main problem in using the offset operation is, that it does not preserve the rationality of a surface. In the case of planar curves there exist several publications which are devoted to rational curves

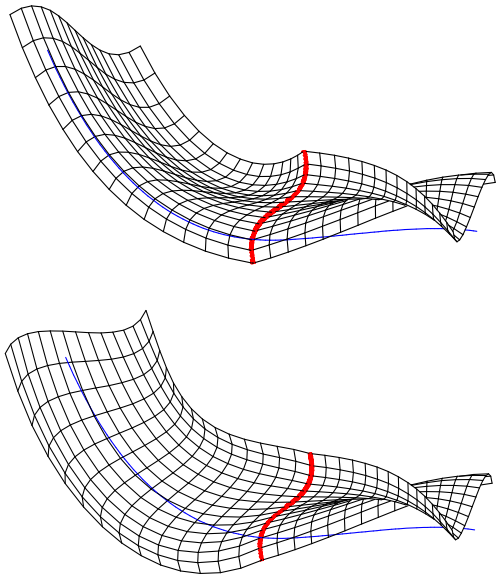

Figure 7: Rational sweeping surfaces with G^0- and G^1-continuity along the segment boundaries.

with rational offsets, see Reference 15 and the references cited therein. The construction of rational surfaces with rational offsets, however, is more difficult, and a lot of problems are still unsolved. We discuss briefly the sweeping surfaces whose offsets can be generated as sweeping surface of the offsets of their cross section curves.

Theorem 6. *Let* $\mathbf{c}_o(s)$ *be the offset curve of the cross section curve* $\mathbf{c(s)}$ *of* $\mathbf{s}(s,t)$*. The sweeping surface generated with* $\mathbf{c}_o(s)$ *(and the same frame as* $\mathbf{s}(s,t)$*) is an offset surface of* $\mathbf{s}(s,t)$*, if the cross section curve is a circle centered at the spine curve or if the function* $\Omega(t)$ *satisfies*

$$\tau(t)\ \sigma(t) + \dot{\Omega}(t) = 0. \qquad (31)$$

Proof. The normal vector of the sweeping surface $\mathbf{s}(s,t)$ can be computed via $\vec{\mathbf{N}}(s,t) = \mathbf{s}_s(s,t) \times \mathbf{s}_t(s,t)$. Owing the Frenet formulas and the relation (21) we may write the normal vector as

$$\vec{\mathbf{N}}(s,t) = [\ldots]\vec{\mathbf{n}}(t) + [\ldots]\vec{\mathbf{b}}(t) + (c_1(s)\dot{c}_1(s)+c_2(s)\dot{c}_2(s))\,(\tau(t)\sigma(t)+\dot{\Omega}(t))\ \dot{\mathbf{x}}(t).$$

If the coefficient of $\dot{\mathbf{x}}(t)$ vanishes, then the offset curves of the cross section curves generate a offset surface of the sweeping surface. Clearly, profile curves with $c_1(s)\dot{c}_1(s) + c_2(s)\dot{c}_2(s) = 0$ describe a circle centered at the spine curve. □

Equation (31) defines a remarkable class of moving frames which have been studied in several publications[8, 12, 16, 18]. From (28) one may conclude that the derivative vectors of the frame are parallel to the tangent vector of the spine curve. These frames are called *rotation minimizing frames* (RMF); they possess many interesting features. The RMF of a cubic PH spline automatically generates a G^1-sweeping surface, because (27) is fulfilled. Sweeping surfaces which are generated with the RMF have curvature line parametrization and their offset surface can be computed via the planar offset curves of the cross section curves. If the cross section curve is a straight line, the corresponding sweeping surface is a developable. Unfortunately the RMF of a cubic PH curve is generally not rational. A rational approximation scheme for the RMF of PH cubics and a geometrical discussion of the corresponding sweeping surfaces, including convexity criteria, will be presented in a separate paper[11].

An example is shown in Figure 8. The left figure shows a cubic PH spline curve with 4 segments (black curve). This curve has been obtained by converting the underlying thick grey curve into a cubic PH spline. In addition to both curves, the boundary points of the PH cubics and the associated unit tangents (dashed lines) have been drawn. The sweeping surface in the second picture has been generated by a rational approximation of the RMF which leads to rational G^1 spline surfaces.

Acknowledgement

The research of the second author was done while he was visiting the Department of Ship Building and Marine Engineering at the National Technical University of Athens, Greece. The financial support of this visit by the European Union through the HCM programme, network 'FAIRSHAPE', and the hospitality of his host, Professor P. Kaklis at Athens, are gratefully acknowledged.

REFERENCES

1. Albrecht, G., and Farouki, R.T., Construction of C^2 Pythagorean-hodograph interpolat-

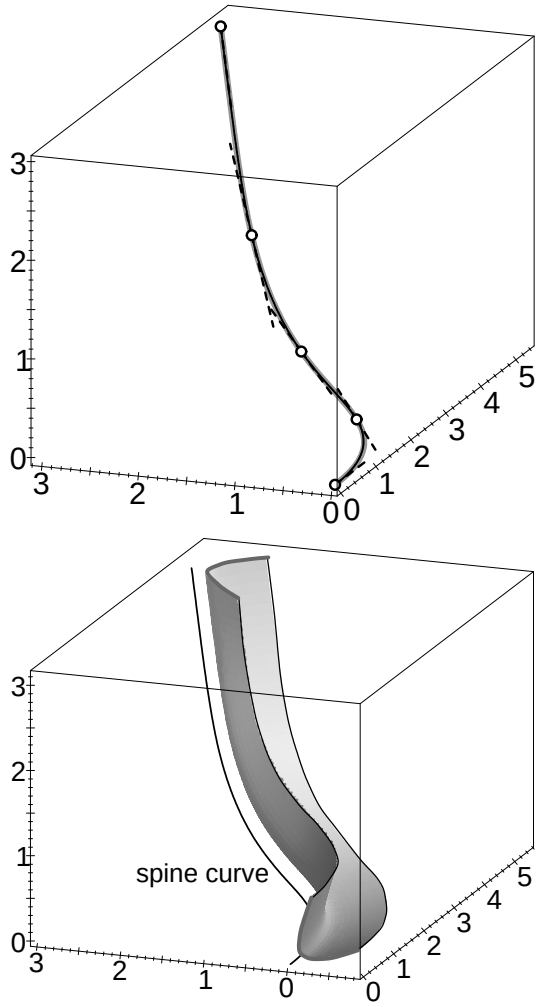

Figure 8: Rational PH spline curve (top) and a sweeping surface (bottom) which is generated by a rational approximation of the rotation minimizing frame.

ing splines by the homotopy method, *Adv. Comput. Math.*, 1996, **5**, 417-442.

2. Dietz, R., Hoschek, J., and Jüttler, B., An algebraic approach to curves and surfaces on the sphere and on other quadrics, *Comput. Aided Geom. Design*, 1993, **10**, 211-229.

3. Farouki, R.T., and Neff, C.A., Hermite interpolation by Pythagorean hodograph quintics, *Math. Comput.*, 1995, **64**, 1589-1609.

4. Farouki, R.T., and Sakkalis, T., Pythagorean hodographs, *IBM J. Research and Development*, 1990, **34**, 736-752.

5. Farouki, R.T., and Sakkalis, T., Pythagorean–hodograph space curves, *Adv. Comput. Math.*, 1994, **2**, 41-66.

6. Farouki, R.T., and Shah, S., Real-time CNC interpolators for Pythagorean–hodograph curves, *Comput. Aided Geom. Design*, 1996, **13**, 583-600.

7. Gravesen, J., Adaptive subdivision and the length of Bézier curves, *Comput. Geom.*, 1997, **8**, 13–31.

8. Guggenheimer, H.W., Computing frames along a trajectory, *Comput. Aided Geom. Design*, 1989, **6**, 77–78.

9. Hoschek, J., and Lasser, D., *Fundamentals of Computer Aided Geometric Design,* AK Peters, Wellesley MA, 1993.

10. Jüttler, B., Generating Rational Frames of Space Curves via Hermite Interpolation with Pythagorean Hodograph Cubic Splines, in *Differential/Topological Techniques in Geometric Modeling and Processing'98*, eds. D.P. Choi, H.I. Choi, M.S. Kim and R.R. Martin, Bookplus press, Seoul, South Korea, 1998, 83–106.

11. Jüttler, B., and Mäurer, C., Rational approximation of the rotation minimizing frame using Pythagorean-hodograph cubics, in preparation.

12. Klok, F., Two moving coordinate frames for sweeping along a 3D trajectory, *Comput. Aided Geom. Design*, 1986, **3**, 217-229.

13. Kreyszig, E., *Differential geometry,* Oxford University Press, London, 1964.

14. Meek, D.S., and Walton, D.J., Geometric Hermite interpolation with Tschirnhausen cubics, *J. Comp. Appl. Math.*, 1997, **81**, 299–309.

15. Pottmann, H., Rational curves and surfaces with rational offsets, *Comput. Aided Geom. Design*, 1995, **12**, 175-192, 1995.

16. H. Pottmann, M. Wagner, Contributions to Motion Based Surface Design, *International Journal of Shape Modelling*, to appear, 1998.

17. Wagner, M., and Ravani, B., Curves with Rational Frenet–Serret motion, *Comput. Aided Geom. Design*, 1997, **15**, 79–101.

18. Wang, W., and Joe, B., Robust computation of the rotation minimizing frame for sweep surface modeling, *Comput.–Aided Design*, 1997, **29**, 379–391.

19. Wunderlich, W., Algebraische Böschungslinien dritter und vierter Ordnung, *Österr. Akad. Wiss., Math.-naturw. Kl., S.-Ber., Abt. II*, 1973, **181**, 353-376.

Bert Jüttler studied Mathematics at the Universities of Technology in Dresden and Darmstadt. He graduated as a Diplom–Mathematiker in 1992 and he gained a PhD in 1994, both from Darmstadt. From 1994 to 1996 he was a postdoctoral research assistant in Darmstadt and at the University of Dundee, Scotland. Currently he is a Lecturer at the Department of Mathematics, Darmstadt University of Technology. His research interests include Computer Aided Geometric Design, Robotics and Kinematics.

(Photograph is attached.)

Christoph Mäurer studied Applied Mathematics at the University of Technology, Darmstadt, Germany. He graduated as a Diplom–Mathematiker in 1994 and gained a PhD in 1997. Since 1997 he was a post–doctoral research assistant at the Centre of Applied Mathematics in Darmstadt and at the Ship Design Laboratory of the National Technical University Athens, Greece. Currently he is employed at the Numerical Simulation Department of TWT, Neuhausen, Germany. His research interests are in Geometric Design and CAD/CAE.

(Photograph is attached.)